Materials and Design 160 (2018) 1305–1321

Contents lists available at ScienceDirect

Materials and Design

journal homepage: www.elsevier.com/locate/matdes

Mechanical properties of sandwich composites with 3d-printed auxetic and non-auxetic lattice cores under low velocity impact

Shaoyu Hou[a,*], Tiantian Li[a,b], Zian Jia[a], Lifeng Wang[a,*]

[a]Department of Mechanical Engineering, State University of New York at Stony Brook, Stony Brook, New York 11794, United States
[b]Department of Engineering, University of Cambridge, Cambridge CB2 1PZ, UK

HIGHLIGHTS

- Auxetic core exhibits lower energy absorption capacity but superior robustness and durability compared with non-auxetic design.
- Only if the impact energy is appropriate will the auxetic panel yield best performance in mitigating impact load.
- The robust auxetic core shows same deformation pattern under various impact energy, and thus stabilizes face sheet penetration occurrence.
- The durable auxetic core remains intact after multi-cycle impacts, and correspondingly grants lattice composites consistent performance.

GRAPHICAL ABSTRACT

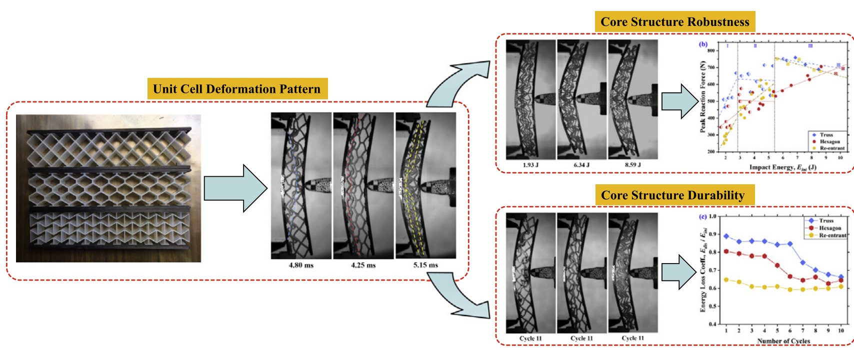

ARTICLE INFO

Article history:
Received 24 August 2018
Received in revised form 1 November 2018
Accepted 1 November 2018
Available online 16 November 2018

Keywords:
Auxetic
Lattice
Reliability
Robustness
Durability
Low velocity impact

ABSTRACT

This work presents a comparative study on the reliability of auxetic (re-entrant honeycomb) and non-auxetic (diamond lattice and conventional honeycomb) lattice composites. The analyzed specimen consists of two unidirectional carbon fiber reinforced composite (CFRP) face sheets and a 3D-printed polymeric core. Low velocity impact tests are conducted first to characterize the unit cell deformation pattern, and we further explore its influence on core structure behavior as well as sandwich panel performance. It is found that the re-entrant topology exhibits lower energy absorption capacity but superior robustness and durability. Consequently, the re-entrant panel performs best in both force mitigation and energy dissipation, provided that the impact energy is appropriate. Furthermore, employing re-entrant core not only stabilizes the occurrences of the face sheet penetration as the impact energy increases, but also grants the sandwich panel consistent behaviors under multi-cycle impacts. These unique performances are due to the global instability of the auxetic structure, which yields more compliant deformation and less stress concentration. Resultant discrepancies shall be interpreted with the sandwich core deformation for validation. These findings pave the way for developing new class of auxetic lattice composites, especially under cyclic loading conditions, through a combination of rational design and 3D printing.

1. Introduction

Sandwich composites used to be assembled with two stiff face sheets for resisting external loads and an embedded cellular core to increase the moment of inertia. Meriting the high specific modulus

* Corresponding authors.
E-mail addresses: Shaoyu.hou@stonybrook.edu (S. Hou), tl484@cam.ac.uk (T. Li), Zi-an.jia@stonybrook.edu (Z. Jia), Lifeng.Wang@stonybrook.edu (L. Wang).

https://doi.org/10.1016/j.matdes.2018.11.002
0264-1275/

and strength, they find applications in many fields, such as aerospace, automotive, marine and energy industry [1]. Compared with changing the thin face sheet, editing the core structure provides more flexibilities in tailoring sandwich panel performance, and of particular interest are the architected auxetic structures, which shrink (expand) laterally under uniaxial compression (stretch). Interestingly, feasible manufacturing approaches first usher the auxetic foam [2] into rapid developments, albeit the auxetic lattice (re-entrant honeycomb [3]) is realized earlier. Thanks to the additive manufacturing, many newly designed auxetic topologies can be built and analyzed. With the two-dimensional (2D) chiral, double-arrowhead and missing-rib lattice studied, community further explores the auxetic effect in three-dimension [4,5], gradient configuration [6,7] as well as multi-material system [8,9]. The potential of auxetic lattice composites has been dramatically broadening.

Employing auxetic topology yields many novel behaviors, such as enhanced indentation resistance and shear modulus [10]. Comparative studies are conducted extensively to investigate the resultant discrepancies in mechanical performance. Scarpa et al. [11] find that the auxetic polyurethane (PU) foam exhibits lowered stiffness but improved structural integrity, binging noticeable crushing resilience. Jiang et al. [12] achieve both higher energy dissipation and better force mitigation by adding auxetic reinforcements in PU-filled textile composites. However, tests on polymer-filled auxetics [13] suggest that the strain rate effect brings up to 70% deviations on their performance. Realizing that the intricate foam core is too cumbersome to quantify the contribution from auxetic network [14], researchers turn to lattice composites with 2D in-plane core configuration (lateral load) for clarity [15]. Numerical studies conducted by Qi et al. [16] successfully reveal the mechanism underlying the enhanced ballistic resistance of the re-entrant honeycomb. Similar analyses from Liu et al. [17] demonstrate that the re-entrant design responds faster to the crushing load but absorbs lower energy eventually. Moreover, Zhou et al. [18] find that varying cell wall thickness affects cell deformation pattern significantly, and results from Li and Wang [19] illuminate the importance of compatible face sheet material. Recently, Sarvestani et al. [20] present a comprehensive analysis on the re-entrant panel. Like those findings reported by Yang et al. [21], they all recommend auxetic design for impact protector since it not only absorbs higher impact energy, but also lowers peak reaction force. It can be found, majority of these works still study multi-layer auxetic structures. They are persuasive for addressing the network effect, but the shock front phenomenon [17,22] makes it hard to characterize the unit cell deformation pattern, not to mention interpreting the resultant mechanical performance from it. Furthermore, all these literatures focus on one specific failure mode of the sandwich panel, i.e. cell collapse [13,17,18,21], facing damage [19,20] or panel perforation [15,16]. The conversion between these phenomena has yet to be discussed. Indeed, it is of great importance to present this transition and reveal the influence of core structure robustness, realizing that the same panel shall experience various loading conditions in practice.

This consideration also raises another concern. Sandwich composites are designed for sustaining load, thus better to be reusable. Great endeavors have been devoted to investigating their performance under cyclic loading. On the one hand, the fatigue behavior of foam cored sandwich composites has been investigated thoughtfully. Besides the conventional analysis on the influence of loading frequency f [23], stress ratio $R = \sigma_{\min}/\sigma_{\max}$ [24], load level $r = \sigma_{\max}/\sigma_{ult}$ [25], and core [26] as well as face sheet [27] property, many literatures are presented to address a bunch of special issues, e.g. modifying load type [28] or sequence [29], varying ambient temperature [30], altering core junction type [31]. Some advanced topics, such as failure mode conversion [32], effects of preset core damage [33] and cyclic impact [34], are also discussed. An exhaustive review can be found in [35]. Bezazi and Scarpa conduct pioneer work to explore the fatigue behavior of auxetic PU foams. They find the auxetic design exhibiting severer rigidity loss but much higher energy dissipation [36] as well as improved fatigue resistance [37]. Lisiecki et al. [38] examine the influence of fatigue load on structural hardness and report that the auxetic foam yields larger thickness reduction but enhanced indentation resistance. Zhou et al. [39] further analyze the performance of PU-filled textile composite under cyclic loading. Filtered force curves indicate that employing auxetic reinforcements attenuates the transmitted load, and most importantly, yields stable performance under multi-cycle impacts. On the other hand, lattice composites with 2D out-of-plane core configuration (axial load) are drawing increasing attentions. Jen's group [40-42] presents a comprehensive study on the fatigue behavior of adhesively bonded aluminum sandwich panels. They recommend combining local stress parameters for predicting failure initiation. Belouettar and Abbadi et al. [43] study Aluminum/Nomex honeycomb composite and find that the L-orientation core is more suitable for sustaining fatigue load. Subsequently, a modified lifetime predictive model is proposed to capture this discrepancy [44] with the influence of preset skin defect discussed in [45]. Some advanced topics, such as varying core orientation between L and W [46], preset interfacial debonding [47], analytical model developments [48] and time-temperature superposition law [49], further reinforce our understandings on the fatigue behavior of sandwich composites. It is well-accepted, lattice composites with out-of-plane configuration carry flexural load by both shearing core structures [50] and buckling cell walls [14]. Thus, the dominant failure mode is either interfacial debonding or wall cracking, and the influence of core topology is commonly neglected. This is not the case, however, for lattice composites with in-plane configuration. To the knowledge of the authors, the fatigue behavior of non-auxetic lattice structures has been investigated analytically [51], numerically [52] and experimentally [53], whereas the durability of the auxetic lattice is rarely discussed, let alone their influence on sandwich panel performance.

The immense potential of employing auxetic topology in sport applications [21,54,55] is urging us to investigate the reliability of auxetic lattice composites. In this work, three designed core structures (diamond lattice, conventional honeycomb, and re-entrant honeycomb) were fabricated using additive manufacturing. They were adhesively bonded with two unidirectional CFRP face sheets and tested under dynamic three-point bending condition. We first loaded three types of lattice composites with close incident velocities to discuss the divergent cell deformation pattern, and then impacted them under various velocities as well as multiple cycles to explore the influence of core structure robustness and durability, respectively. The peak reaction force, energy loss coefficient and maximum back facet deflection were quantified and compared accordingly. All the resultant discrepancies shall be interpreted with the core deformation differences for validation.

2. Material and methods

2.1. Core design

In-plane behavior of lattice composites is strongly affected by the core structure [15]. Here, three types of core topologies: diamond lattice (truss), conventional honeycomb (hexagon) and re-entrant honeycomb (re-entrant), were studied. The main purpose of this work is to identify the cell deformation pattern and investigate how they affect sandwich panel performance. Therefore, 2D topology was selected, and the volume fraction was set to be 20%. Three types of cellular structures are fixed to have the same dimension of the unit cell, i.e., 9 mm by 9 mm. This approach provides a more straightforward observation of the divergent unit cell deformation pattern. It should be acknowledged that this design also grants different slenderness ratio to the vertical strut of each topology, which in turn requires divergent Eulerian buckling load. Fig. 1 shows three designed unit cells with the dimension summarized in Table 1. Theoretically, the volume fraction can be estimated with

$$V_f = \frac{t(H/L+2)}{2\cos\theta L(H/L+\sin\theta)} \quad (1)$$

The tested sandwich core was assembled by twenty unit cells (10 by 2), and extra twenty 4.5 mm by 0.5 mm by 10 mm thin plates were implemented for applying adhesive.

2.2. Sample preparation

Fig. 2 shows one prepared sandwich panel. Each sample was adhesively bonded with epoxy adhesive DP420 (3 M Scotch-Weld). Unidirectional CFRP was selected as the face sheet material, and we aligned its longitudinal direction with 1-direction. The designed core structure was fabricated using a 3D printer (Objet Connex260, Stratasys) with digital material FLX9795-DM. To eliminate the effect of the anisotropic nature from additive manufacturing, all samples were fabricated along the same orientation, and then left in room temperature at least seven days for the saturation of curing. Moreover, we herein focused on sandwich panels with W-orientation core arrangement [43]. L-type sandwich core exhibited global bending behavior without unit cell deformation and hence was not reported. The dimension and material property of each component were summarized in Table 2. Detailed material characterization can be found in our previous works [56,57].

2.3. Dynamic three-point bending test

Impact tests were conducted on a modified Split-Hopkinson Pressure Bar (SHPB) system. Fig. 2.a shows the configuration. The striker inside the gun barrel was accelerated by the compressed air from the gas tank to fire the impactor. Two photoelectric sensors at the end of the barrel output signals into a digital oscilloscope (DSO-X 2004A, Agilent Technologies) to trigger the high-speed camera system (FASTCAM SA1.1, Photron). The images were recorded at 20 kHz frame rate (0.05 ms/frame) and collected by the FASTCAM Viewer automatically.

Fig. 2.b gives a zoomed view of the auxetic lattice composite before impact. Some used terminologies are defined accordingly.

Table 1
Dimensions of the designed core topology (unit: mm).

Parameter	Core topology		
	Truss	Hexagon	Re-entrant
Angel, θ	45°	30°	−30°
Thickness, t	0.67	0.71	0.50
Length, L	6.37	5.20	5.20
Height, H	0	1.90	7.10

Two soft fixtures were used to hold the sandwich panel for three-point bending condition. The span was set to be 72 mm, and we implemented another speckle pattern in the middle of the back face sheet for recording deflection. The profile of the impactor has considerable influence on sandwich panel performance [16]. In this study, hemispherical projectile with nose radius 3.2 mm was selected. It ensures that the panel deformation is bending rather than compression and prevents the front face sheet from penetration before core structure deforms. Meanwhile, the impactor is 63.5 mm wide in 3-direction, which is much larger than that of the sandwich panel (10 mm). The layer-by-layer fabrication process produces tapered cell walls. This large value not only helps to yield 2D deformation pattern, but also eliminates the edge effect. Furthermore, due to the constraint from adherends, only the second layer can be regarded as an active layer compared with multi-layer configuration [16]. We employed this simplified design to idenfity the influence of core structural micro-dynamics [11] by avoiding the shock front phenomenon [17,22]. In general, all samples experienced symmetric deformation throughout the investigation, and no CFRP delamination or interfacial debonding was observed. It should be noted that the current experimental setup may not yield a standard three-point-bending condition. The three-point-bending fixture is selected here to make sure that the back face sheet could deform under impact load. The maximum face sheet deflection was considered as an important index for evaluating sandwich panel performance [19], and we will use it in the following discussion for comparing the influence of core topologies.

2.4. Data processing

Impactor displacement and back face sheet deflection were first read from the speckle pattern with Digital Image Correlation (DIC)

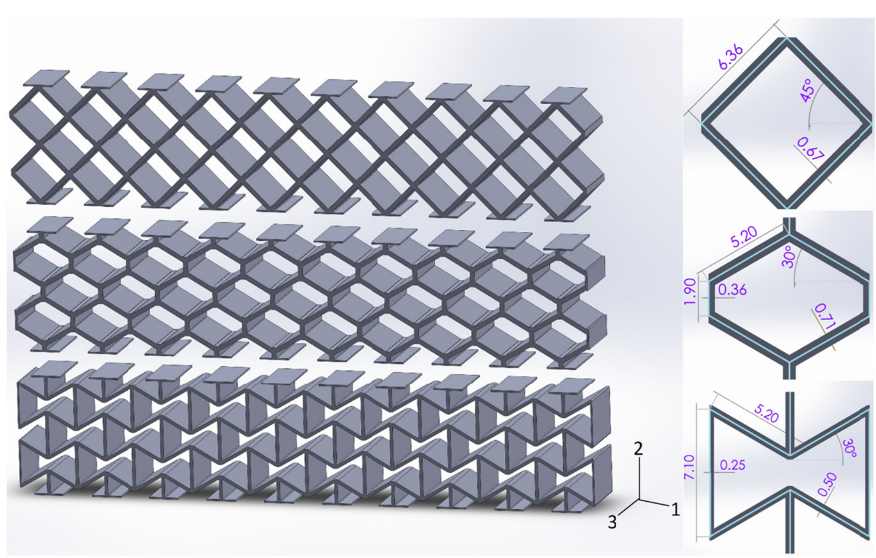

Fig. 1. Designed sandwich core and unit cell for diamond lattice (truss), conventional honeycomb (hexagon) and re-entrant honeycomb (re-entrant), respectively (unit: mm).

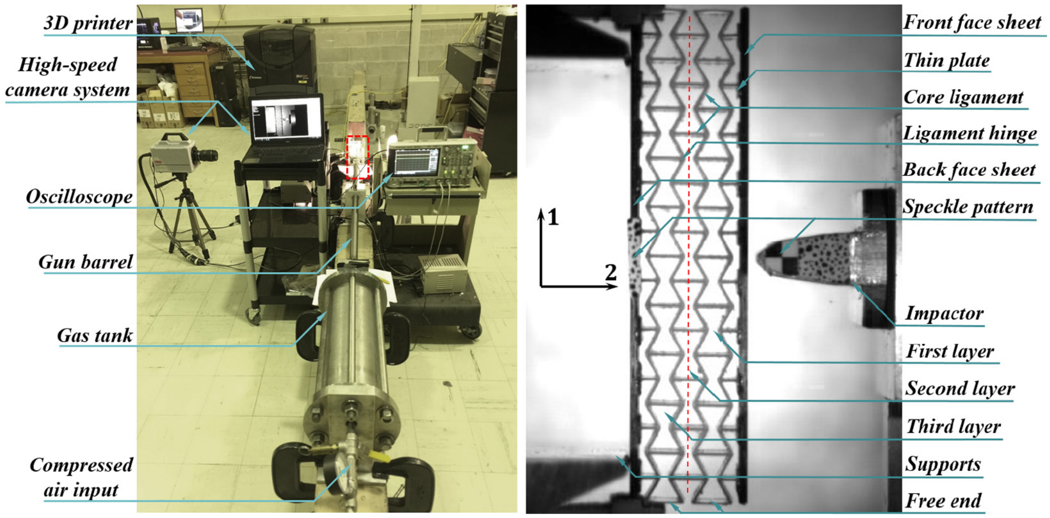

(a) Global (b) Zoomed

Fig. 2. Experimental setup of the dynamic three-point bending test.

technique (VIC-2D, Correlated Solution Inc.). After that, velocity and acceleration could be calculated by differentiating the displacement history, and we defined the instantaneous inertial force of the impactor as the reaction force. Accompanied with the sandwich core deformation, lots of noises are introduced when acquiring this force curve. Thus, a suitable signal processing method is preferred, or else the force trend shall be overwhelmed by the perturbation [39,58]. Here, we took advantage of Fast Fourier Transform (FFT) with a low-pass filter to smooth the response force curve. Based on MIL-STD-883F Method 2002.4, the cut-off frequency for all scenarios should be larger than 0.5 kHz. In the following discussion, results filtered by 1.0 kHz were used, and our conclusions had been further examined with employing three different cut-off frequencies, i.e. unfiltered, 1.5 kHz and 2.0 kHz, respectively. It is worth noting that using the filter also removes the perturbation from core ligament fracture, which occurs within 0.05 ms (1 frame) and is localized. But its effect on the global force trend is kept, showing the influence of varying core topologies.

Moreover, we quantified three parameters to compare the mechanical performance. The maximum back face sheet deflection and the peak reaction force were read from the corresponding curves directly, and the dissipated energy could be evaluated through

$$E_{dis} = E_{ini} - E_{res} = \frac{1}{2} \cdot m \cdot \left(V_{ini}^2 - V_{res}^2\right) \quad (2)$$

in which, m is the mass of the impactor, 0.333 kg. V_{ini} and V_{res} are the impactor velocities when it reaches and disconnects from the front face sheet, respectively. The same approach has been implemented successfully previously [57] for evaluating the performance of CFRP under dynamic three-point-bending load. Indeed, current experimental setup is more like a horizontal "drop-weight" impact test rather than a conventional SHPB system. In drop-weight test, researchers commonly use the kinetic energy loss (area beneath the force-displacement curve) to define the energy dissipation [12,20]. Meanwhile, compared to the SHPB configuration, current system provides more information on the behavior of the impactor, which is of particular interest for engineers aiming at designing protective pad. Finally, the energy loss coefficient [59] could be calculated using E_{dis}/E_{ini}. To the best of the authors' knowledge, the same experimental setup as well as the sandwich panel configuration has not been reported in other open literatures. Thus, we shall focus our investigation on the influence of altering core topology. All the comparisons are made between these three types of lattice composites. A comprehensive investigation on the influence of the test method will be left as a future work.

3. Results and discussion

3.1. Influence of the cell deformation pattern

Fig. 3 summarizes the recorded curves from three types of lattice composites under close incident velocities. As can be seen, employing re-entrant core yields much larger ultimate impactor displacement (15.90 mm in Fig. 3.a). Meanwhile, the re-entrant panel also takes longer time (5.15 s) to absorb the impact energy and gives the highest post velocity (2.83 m/s) in Fig. 3.b. They imply that the

Table 2
Dimension and material property of the tested lattice composite.

Component	Dimension			Material property			
	1-direction (mm)	2-direction (mm)	3-direction (mm)	Young's modulus (MPa)	Poisson's ratio –	Strength (MPa)	Density (kg/m^3)
Core	90	19	10	5.5	0.37	1.7	1157
Face sheet	90	1.5	10	94000[1]	0.0226[1]	1400	1475
Adhesive	–	–	–	–	–	31[2]	1140

[1] Longitudinal modulus and Poisson's ratio.
[2] Shear strength.

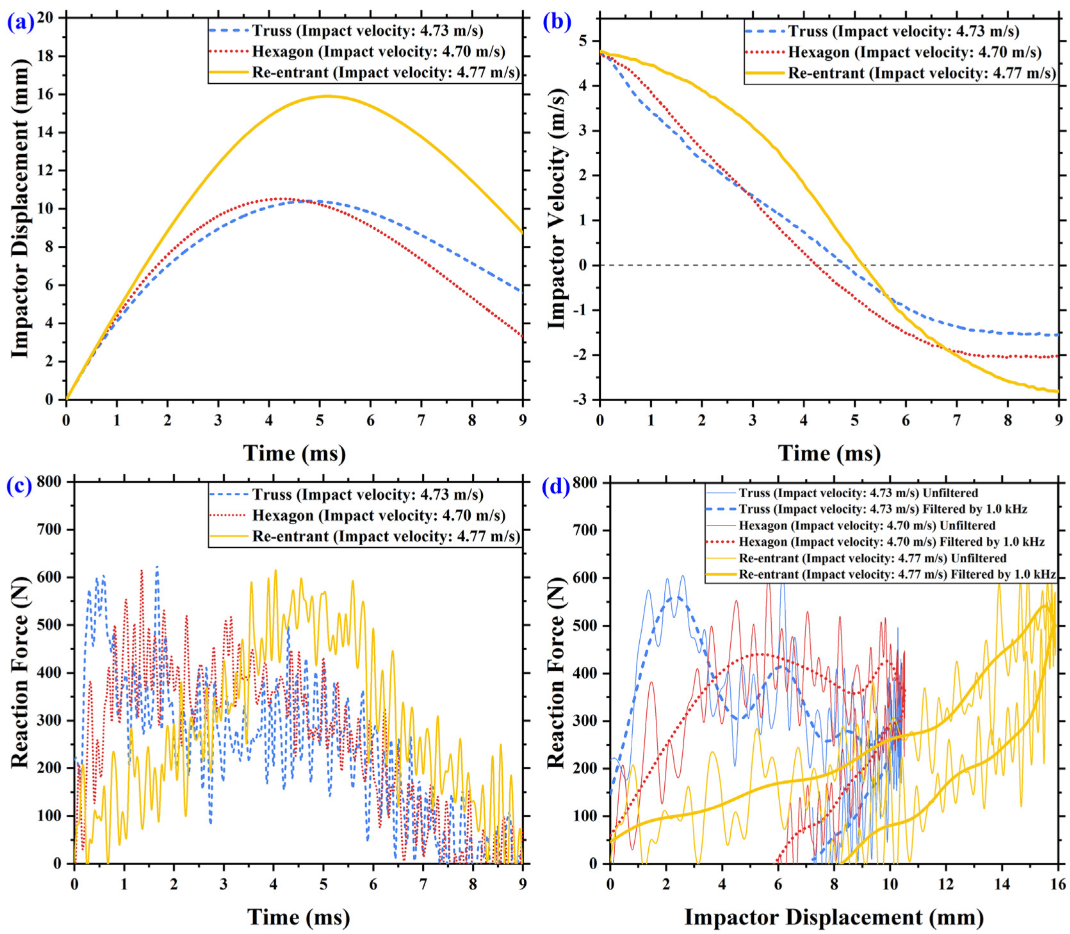

Fig. 3. Typical curves of the impactor from three tested lattice composites. They are for (a) displacement versus time, (b) velocity versus time, (c) unfiltered reaction force versus time, (d) filtered reaction force versus displacement, respectively.

mean energy absorption rate (J/s) of the re-entrant design is relatively low, and more impact energy has been released eventually. By contrast, the truss panel performs best in dissipating energy, and the hexagon one appears to be the most efficient candidate. The unfiltered reaction force fluctuates heavily in Fig. 3.c, and the truss design shows the highest flexural stiffness with the hexagon exhibiting intermediate performance. By using FFT with low-pass filter, filtered as well as unfiltered force curves are plotted against the impactor displacement in Fig. 3.d. The filtered curve can follow the trend quite well and is much smoother. We find that the peak reaction force in the truss and re-entrant panel are close, but larger than that of the hexagon. Additionally, both truss and hexagon exhibit suppressed reaction force until the impact energy is fully absorbed, whereas the loading curve of the re-entrant panel depicts monotonic increasing trend with three minor perturbations.

3.1.1. Resultant velocity differences

These discrepancies are from employing different core topologies. Unlike conventional analysis discussing perturbed force trends, we shall elaborate the influence of the cell deformation pattern by interpreting the recorded velocity curves. A supplementary discussion on the force and displacement trend is enclosed in Appendix A.

Fig. 4 plots the velocity difference ΔV between the impactor and the back face sheet midspan for each design. To a solid core ($V_f = 100\%$), the velocity difference used to vanish soon after some continuous, attenuated oscillations. Therefore, it is the core structure deformation that induces the aberrant behaviors. As shown in Fig. 4, the expected first overshooting disappears from the re-entrant panel. It suggests that the re-entrant design performs better in attenuating the transmitted impact load, which has also been observed from simulating drop weight scenario [15] and for auxetic textile composites [39]. Subsequently, all panels yield heavy oscillations, introducing

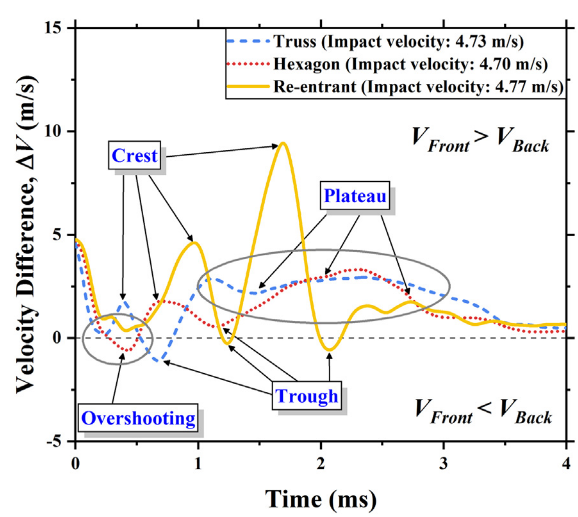

Fig. 4. Velocity difference, ΔV, between the impactor and back face sheet midspan from three tested lattice composites. The calculated impact energy ($E_{ini} = mV_{ini}^2/2$) is 3.74 J, 3.69 J and 3.80 J for truss, hexagon and re-entrant, respectively.

at least one crest and a clear plateau before stabilizing the force transmission (4.00 ms).

They are the consequence of core structure instability. Fig. 5 is selected to display those moments for overshooting, trough, end of plateau, end of absorption and end of impact, respectively. As can be seen, both truss and hexagon can establish stable force transmission path immediately (Fig. 5 (T1,H1)). With the transmitted load increasing, ligaments near two free ends buckle first, and thus the back face sheet bends suddenly (Fig. 5 (T2,H2)). Interacting with the dynamic inertial effect, this mechanism produces a crest and the following trough for these two panels. Interestingly, there is one extra oscillation before plateau in the re-entrant panel. The auxetic effect folds core ligaments towards the impact area (Fig. 5.R1). Ligament hinges may contact each other temporarily. As a result, the back face sheet accelerates, lowering the velocity difference. This status is unstable. Re-entrant cells tend to evolve into interlaced pattern (Fig. 5.R2) for stabilizing the force transmission, which introduces the second crest and trough. An analytical investigation on this behavior can be found in [18]. After the oscillation, more ligaments buckle inside the truss and hexagon core to stabilize the transmitted force, producing localized hinge-rotation and snap-through pattern, respectively (Fig. 5 (T3,H3)). The interlaced pattern, on the other hand, occurs globally and also leaves the re-entrant core some ligaments to buckle (Fig. 5.R3). Stabilizing the transmitted force freezes the velocity difference. Far fewer buckled ligaments thus bring the re-entrant panel a much shorter plateau. Therefore, we think the auxetic effect

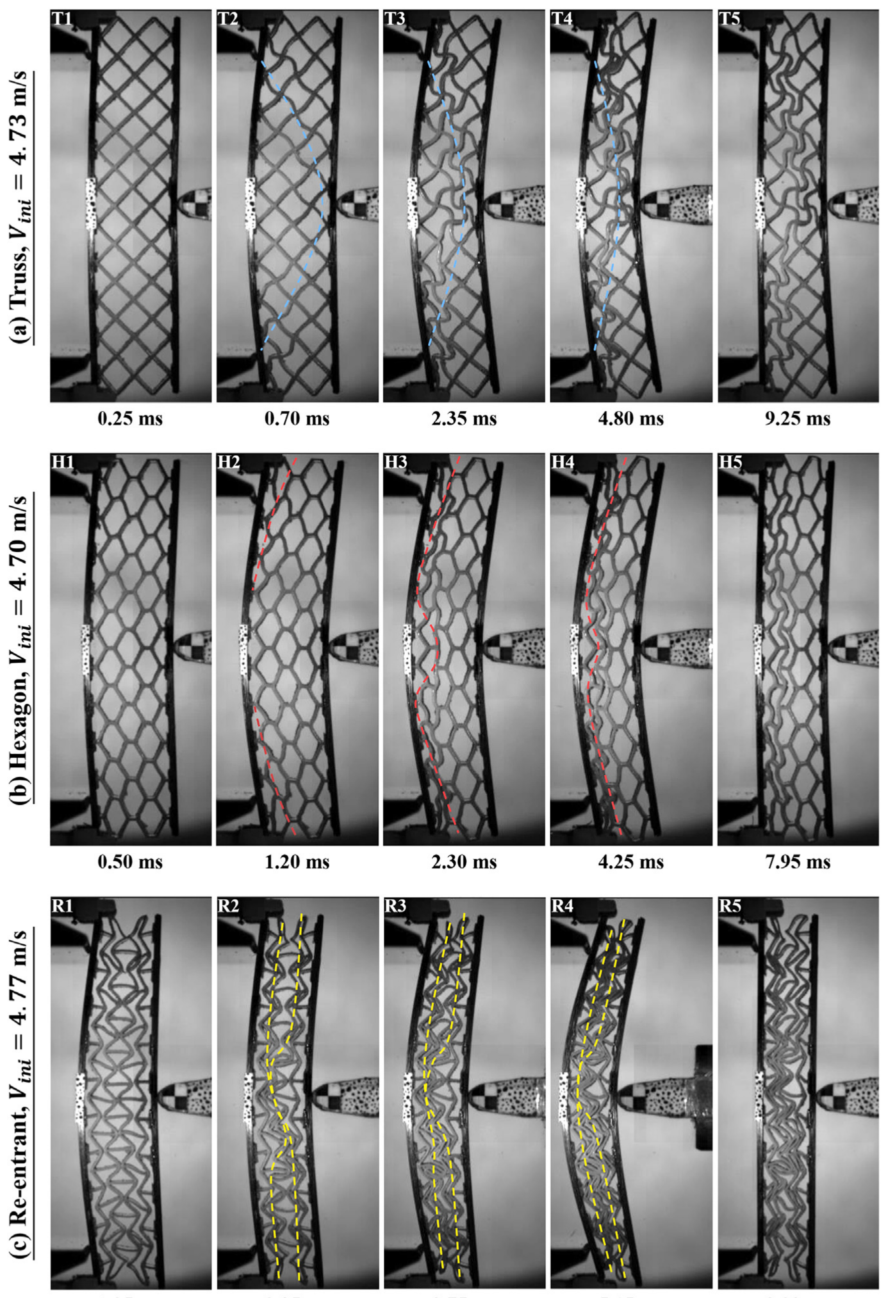

Fig. 5. Snapshots of three tested lattice composites for truss (T), hexagon (H) and re-entrant (R), respectively. They are selected to show moments in Fig. 4 for overshooting (T1,H1), trough (T2,H2,R1,R2), end of plateau (T3,H3,R3), end of absorption (T4,H4,R4), and end of impact (T5,H5,R5); dash lines are used to indicate the deformation region.

Table 3
Energy composition of the impact process for three tested lattice composites.

Topology	Velocity (m/s)		Deflection (mm)		Energy (J)				
	V_{ini}	V_{res}	D_{front}	D_{back}	E_{ini}	E_{res}	E_{facet}	E_{core} [1]	E_{dis} [2]
Truss	4.73	1.57	3.34	3.14	3.74	0.41	0.27	3.47	3.33
Hexagon	4.70	2.07	4.47	4.47	3.69	0.72	0.51	3.18	2.97
Re-entrant	4.77	2.82	5.33	7.11	3.80	1.34	1.00	2.79	2.46

[1] Impact energy absorbed by the sandwich core, $E_{core} = E_{ini} - E_{facet}$
[2] Impact energy dissipated by the sandwich panel, $E_{dis} = E_{ini} - E_{res}$

behaves like a higher-level instability mechanism. It requires the re-entrant core to deform globally first for establishing a stable force transmission path. This process will inevitably stack some core ligaments, which lose the potential to experience large deformation for absorbing energy subsequently. After that, the deformed auxetic structure acts like other two non-auxetic structures, buckling and densifying the rest of core ligaments to sustain further load.

Furthermore, Fig. 5 (T4,H4,R4) displays the deformed lattice composites when the impact energy is fully absorbed. We can estimate the elastic strain energy collected by the two face sheets with

$$E_{facet} = \frac{1}{2} \cdot K_{facet} \cdot \left(D_{front}^2 + D_{back}^2 \right) \tag{3}$$

where, $K_{facet} = 25.74$ kN/m is the flexural stiffness characterized in Appendix B. D_{front} and D_{back} are the face sheet deflection evaluated through DIC. Table 3 calculates the energy composition for each panel. It can be found that the re-entrant core absorbs least impact energy (2.79 J). Considering that both truss and hexagon panel still own some undeformed unit cells, we believe firmly that the energy absorption capacity of the re-entrant structure is not as good as the other two designs. Similar conclusion has also been drawn from dynamic crushing simulation [17]. This lower energy absorption capacity is mainly due to those stacked core ligaments (marked with yellow line in Fig. 5.R2) resulting from the global instability, and the relatively larger slenderness ratio of the buckled vertical struts in the re-entrant core (Fig. 5 (R2–4)) also contribute. It should be noted that this discrepancy is fundamentally caused by the unique unit cell deformation pattern and may be insignificant when plastic deformation or fracture occurs. Additionally, Fig. 5 (T5,H5,R5) shows that the bent face sheets are almost recovered when the impact ends. In other words, current sandwich panel configuration dissipates majority of the impact energy through the viscoelastic behavior of the core structure. Thus, employing re-entrant topology also degrades the energy dissipation ability, given that the re-entrant panel dissipates least energy (2.46 J) in Table 3 as well. This is counter-intuitive, since many literatures report enhanced energy dissipation ability via employing auxetic core in lattice composites. For example, it postpones face sheet rupture under static loading [19] and brings localized densification in penetration test [16]. The culprit here is the comparatively low energy absorption capacity or, more specifically, the influence of the cell deformation pattern under different loading conditions. We shall address this by discussing the core structure robustness.

3.2. Influence of the core structure robustness

A robust design withstands adverse loading conditions without malfunctioning. To achieve a clear understanding on the core structure robustness, especially its influence on sandwich panel performance, we impacted three types of lattice composites with various impact energy.

3.2.1. Failure mode transition

Fig. 6 shows the deformed sandwich panel under different incident velocities ($E_{ini} = mV_{ini}^2/2$). As anticipated, more ligaments buckle inside the truss and hexagon core for absorbing higher impact energy, producing not only wider, but also severer hinge-rotation and snap-through phenomenon (Fig. 6 (VT1-3,VH1-3)). Interestingly, the deformed region starts to diminish when the impact energy becomes even larger (Fig. 6 (VT3-5,VH3-5)). In contrast, the unique interlaced pattern always emerges from the re-entrant core, no matter how large the impact energy is (Fig. 6 (VR1,VR5). These phenomena imply that the instability mechanism in both truss and hexagon core is more sensitive to the impact velocity. Only after the transmitted force reaches the critical value would the ligament buckling activate, and the power is also restricted by the time for it to develop. The re-entrant structure, conversely, is very robust. It always uses the same deformation pattern to dissipate the impact energy. Like the meritorious force mitigation property, this improved robustness also results from employing compliant auxetic topology [11], but the trade-off is the comparatively low energy absorption capacity. Consequently, the front face sheet of the re-entrant panel ruptures earlier due to the large deflection (Fig. 6 (VT3,VH3,VR3)). However, it is imprudent to claim that this is a disadvantage. On the one hand, comparing to the structural robustness which is governed by the topology, the energy absorption capacity is easier to get enhanced, e.g. adding layers. On the other hand, close examination on Fig. 6 (VT4,VH4,VR4) also reveals some fractured core ligaments in both truss and hexagon panel, even if their face sheets are still intact. It could be regarded as a side effect of the high absorption capacity, which naturally raises the concern of their core structure durability.

3.2.2. Mechanical performance under various impact energy

Therefore, it's the cell deformation pattern that decides core structure robustness, governing energy absorption mechanism, and brings each panel unique mechanical performance. Fig. 7 (a,c,e) compares the filtered reaction force curves for truss, hexagon, and re-entrant panel, respectively. In general, both truss and hexagon produce two crests and an in-between plateau. Crests before plateau in the truss panel are always higher (≈650 N) than those from the hexagon (≈500 N), which says the hexagon core performs better in mitigating peak force. As the energy increases, these two structures buckle more ligaments first, producing the plateau, and start to bend with two face sheets at some moments (>6 J), shifting the crest accordingly. They are not robust however. Excessive impact energy (>9 J), on the contrary, allows fewer ligaments to deform, and hence brings premature face sheet rupture (14 mm). This mechanism also explains the behavior of the re-entrant panel. The auxetic effect folds core ligaments and improves structural integrity [11]. Fully densified re-entrant structure mimics a solid core. Thus, the peak reaction force increases monotonically. Even though the front face sheet ruptures earlier, the superb robustness stabilizes the penetration occurrence (17 mm) regardless of the impact energy. Most importantly, the robust core behavior makes the sandwich panel performance more predictable. For example, we expect that the re-entrant panel

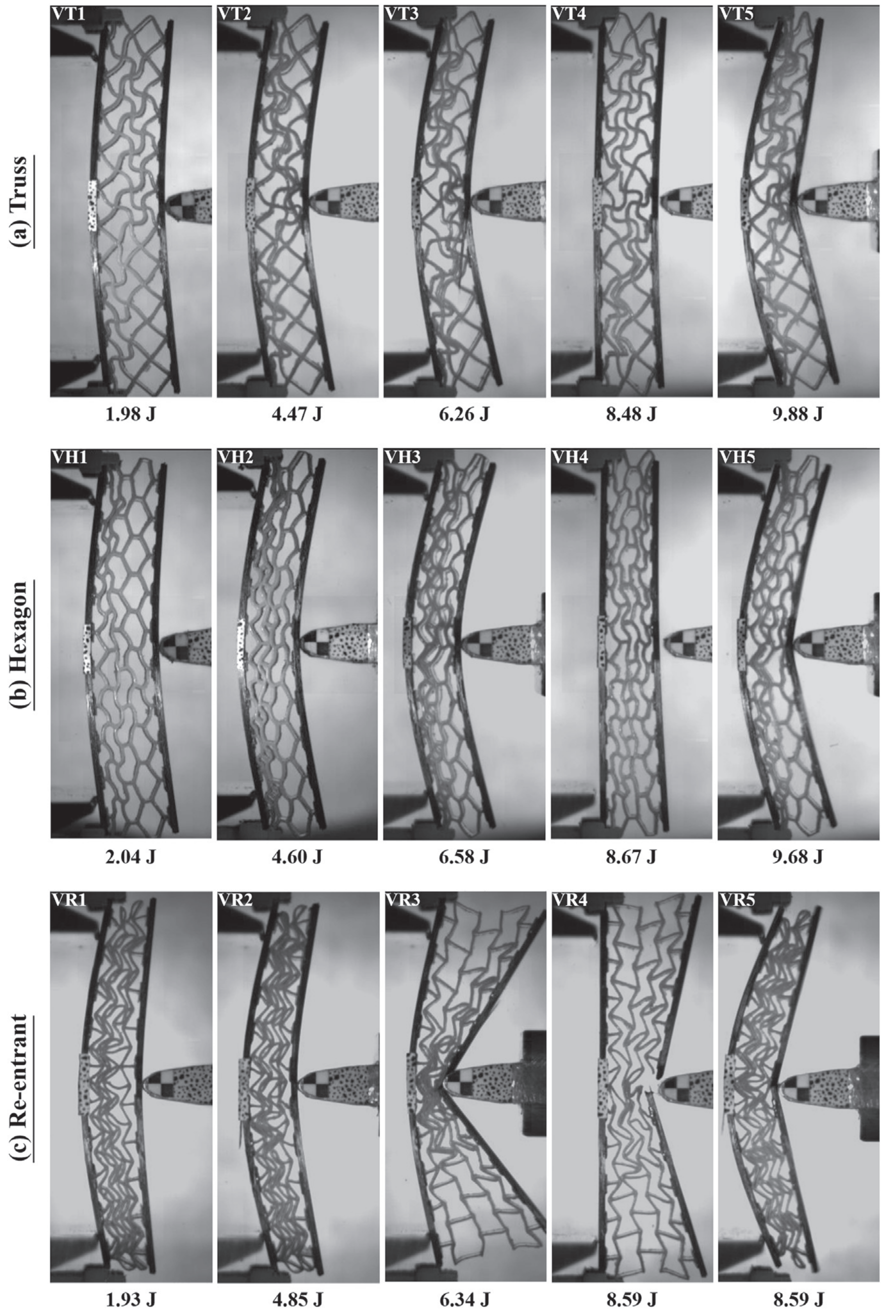

Fig. 6. Snapshots of some tested lattice composites under various impact velocities ($E_{ini} = mV_{ini}^2/2$) for truss (VT), hexagon (VH) and re-entrant (VR), respectively. They are for the moment when the impact energy is fully absorbed (VT1-3,VH1-3,VR1-3), when the impact ends (VT4,VH4,VR4) and when the front face sheet ruptures (VT5,VH5,VR5).

exhibits both raising energy loss coefficient and descending back face sheet deflection as the impact energy decreases, since the global interlaced pattern shall always emerge.

This is easy to get verified. We summarize the peak reaction force, energy loss coefficient and maximum back facet deflection from all scenarios into Fig. 7 (b,d,e). They are categorized into three regions based on the energy absorption mechanism of the re-entrant panel. In the first region (Section I), all three designs utilize core deformation to dissipate most of the impact energy, producing high energy loss coefficient and low face sheet deflection. Meanwhile, given that the re-entrant topology performs best in mitigating impact load [20,21], it yields the lowest peak reaction force. The correlation between energy loss coefficient and back face sheet deflection also prevails in the second region (Section II). For absorbing higher impact energy, fully densified re-entrant core bends with two face sheets, whereas both truss and hexagon core buckle more ligaments. Consequently, the maximum deflection of the re-entrant panel increases significantly while other two designs perform comparatively stable. Furthermore, although the core structure instability perturbs the peak reaction force significantly, the truss panel still yields the highest value, and the re-entrant panel exhibits a steep rising trend intersecting the other two. Increasing impact energy shall break the stiff CFRP soon. The front face sheet of the re-entrant panel ruptures first when entering the third region (Section III). It stabilizes the peak reaction force, dissipates a huge amount of impact energy, and correspondingly boosts the energy

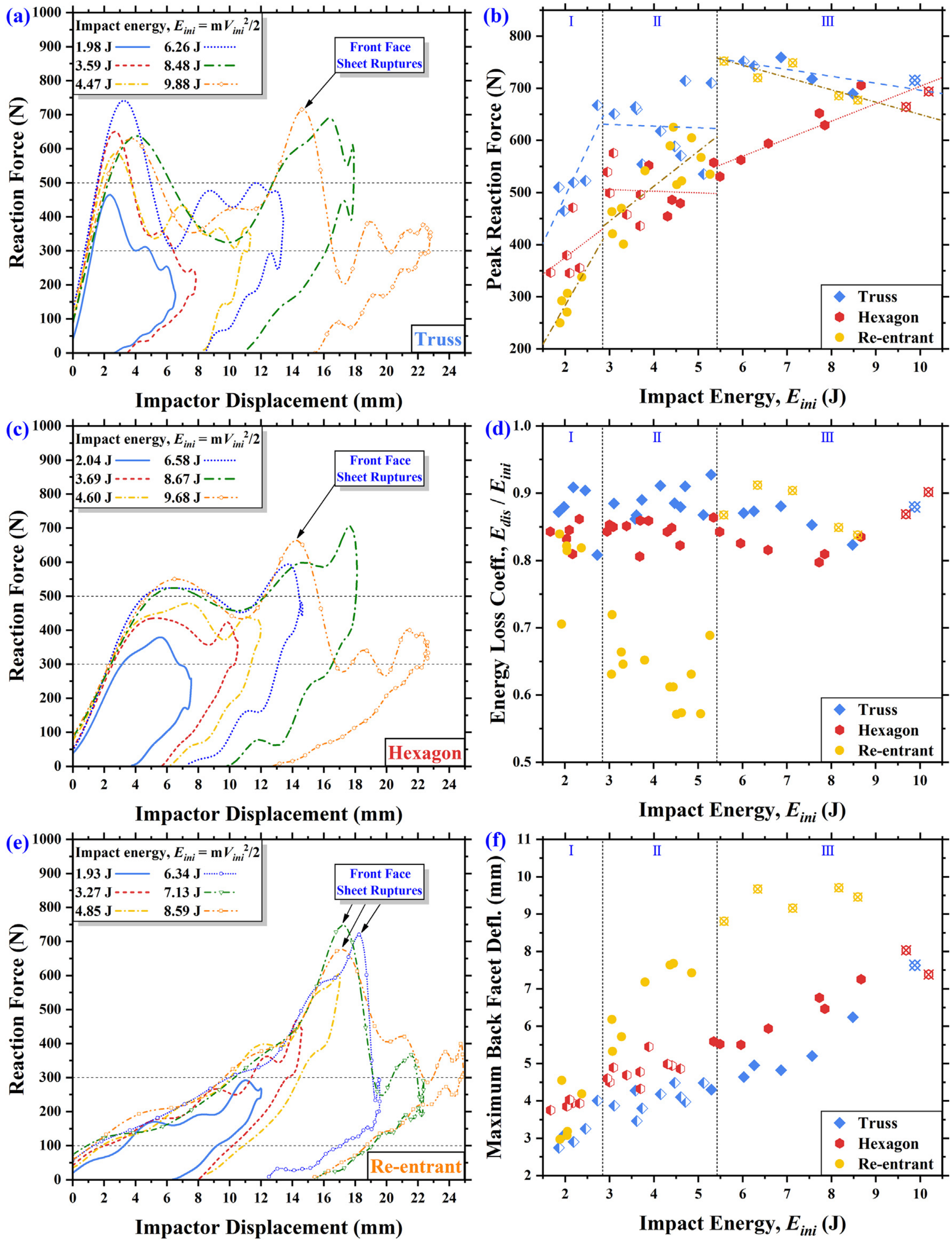

Fig. 7. Filtered reaction force curves and summarized three parameters. Left three are for (a) truss, (c) hexagon, and (e) re-entrant panel, respectively; right three compare the trend of (b) peak reaction force, (d) energy loss coefficient, and (f) maximum back face sheet deflection; crossed symbol indicates the front face sheet ruptures, and half-filled symbol means the value is found before core structure instability; lines in (b) are linear regression for each topology.

loss coefficient. On the other hand, both truss and hexagon core are suffering from robustness issue. Fewer buckled ligaments decrease the energy dissipation and increase the maximum deflection. The peak reaction force, as expected, rises gradually until approaching the limit (≈750 N).

The intersecting trend in Fig. 7 (b,d) not only explains how the core absorption capacity affects sandwich panel dissipation ability, but also helps to address a common conflict in auxetic foams. It is well-accepted that employing auxetic topology dissipates more energy compared with the non-auxetic one. Nevertheless, some researchers observe alleviated response force [60] while others find the impact mitigation property is worsened by employing auxetic topology [61]. A possible explanation could be credited to the lower energy absorption capacity of the auxetic structure. We agree that the auxetic design is good at mitigating impact load. But excessively exerted force (energy) shall densify the structure earlier and then raise the reaction force drastically. This interpretation aligns with the conclusion made by Sarvestani et al. [20]. They recommend increasing volume fraction to keep both high energy dissipation and low peak response force of the re-entrant panel. Besides, alternative explanation also exists. The compliant re-entrant structure is easier to fail in localized densification under high velocity crushing (shock fronts phenomenon [22]). It also introduces a crest to the response force curve in the early stage, but the force value may decrease later [17]. These two interpretations focus on the drawback of the low absorption capacity as well as the compliant structure deformation, convincing us that the auxetic design should be selected and tuned based on the loading condition for the best performance.

3.3. Influence of the core structure durability

With the impact energy increasing, the re-entrant panel ruptures the front face sheet earlier while other two designs fracture core ligaments instead. Lattice composites designed for protective purpose should be reusable, thus either failure mode demands further examination. It motivates us to study their mechanical performance under cyclic impact.

We reload each panel multiple cycles. The incident velocities are close, and the loaded sample was left in the room temperature for one hour to decouple the interaction between core network and material viscoelastic behavior [36]. Meanwhile, since the incident velocity between different cycles shows a slightly increasing trend, we here report two loading scenarios. Results from impact velocity, $V_{ini} = 4.80 \pm 3\%$ m/s (medium, 3.84 J) and $V_{ini} = 5.28 \pm 3\%$ m/s (higher, 4.65 J), are used for discussion. Similar analysis on impact velocity, $V_{ini} = 4.29 \pm 3\%$ m/s (lower, 3.07 J), is provided in Appendix C for validation.

Fig. 8 plots the filtered reaction force versus impactor displacement. Left three are for the medium impact velocity scenario, and the face sheet stays intact. Unlike increasing impact energy, the first crest in both truss and hexagon panel declines gradually. They cannot be stabilized to form a plateau (400 N in Fig. 7 (a,c)), but keep on decreasing until the trend becomes similar to that from the re-entrant panel. It suggests that the core structure changes, which affects the response force mitigation mechanism. By contrast, curves from the re-entrant design are almost overlapped, suggesting consistent sandwich core behaviors. On the other hand, raising impact energy makes it easier to break the face sheet. Right three figures are summarized for the higher velocity scenario. The trend before face sheet rupture is similar to its medium velocity counterpart, but divergence emerges after that. The re-entrant panel still shows resistance to the cyclic impact, whereas both truss and hexagon panel get penetrated subsequently. To compare the mechanical performance resulting from these divergent behaviors, we quantified three parameters into Fig. 9.

3.3.1. Perturbed peak force and progressively damaged core

Fig. 9.a examines the peak reaction force. It is evident that the re-entrant panel yields stable peak values while those from the truss and hexagon panel are perturbed. Initially, the truss panel gives the highest response force, but it decreases immediately. After that, both truss and hexagon show clear rising trend, and all three curves converge and become stable eventually. Similar phenomenon could also be observed from the higher impact velocity scenario in Fig. 9.b.

They are the consequences of progressively damaged core structures. The first three figures in each row of Fig. 10 are selected to show the deformed lattice composite when the peak reaction force occurs. To the truss panel, buckled ligaments in the highlighted area (Fig. 10.CT1) suffer from large deformation and fracture. These damaged cell walls not only enable wider range of structure instability, lowering the peak reaction force, but also enforce the core to deform even severer, inducing more fractured ligaments. The hexagon structure also shows some damaged cell walls (Fig. 10.CH1). It intrinsically suppresses the response force via layered snap-through pattern and hence shows no further peak force mitigation. That is not the case, however, with the cyclic impact continues. Damaged regions grow inside both truss and hexagon core until only one layer of unit cells is left to be intact (Fig. 10 (CT2,CH2)). At this moment, those undamaged ligaments experience stronger boundary condition, and correspondingly require higher critical load to buckle. Thus, they remain straight, and the panel bends as a whole for absorbing residual impact energy, raising the peak force value accordingly. This rising trend shall get suppressed soon, since these intact ligaments will buckle again when the residual impact energy becomes even larger. Fig. 10 (CT3,CH3) displays two further loaded panels, and those under higher impact velocity are shown in Fig. 10 (CT4,CH4). The developed hinge-rotation and snap-through region verify this understanding. Therefore, it is still the cell deformation pattern that decides sandwich panel performance. Fig. 10 (CR1-3) indicates that the same interlaced pattern emerges throughout the cyclic loading test. This pattern occurs globally, introducing less stress concentration compared with the other two. Hence, the re-entrant core stays intact after multiple impacts, showing superb durability, and correspondingly yields constant peak reaction forces. Moreover, one circled ligament in Fig. 10.CR1 also fractures in the early stage. But it neither brings any progressive damage behavior nor affects the performance of the re-entrant panel. This is another advantage of the globalized cell deformation pattern.

3.3.2. Degraded energy dissipation ability

The damaged core structure also degrades the energy dissipation ability. Fig. 9 (c,d) compares the calculated energy loss coefficient for two loading scenarios. Both truss and hexagon exhibit decreasing trend while the re-entrant panel dissipates lower but constant impact energy until the front face sheet ruptures.

Interestingly, the performance of the truss and hexagon panel is also quite stable in the first few cycles, but it gets worse suddenly. For instance, the truss panel experiences a steep decreasing after cycle six, and recall that this is where the peak reaction force converges in Fig. 9.a. It is still the consequence of the core damage evolution. Damaged cell walls shall not affect the energy dissipation significantly, given that the sandwich panel can automatically seek compensation by buckling and fracturing more core ligaments. Nevertheless, when the two face sheets bend further due to the resultant "stronger" core, it is not surprising that larger deflection produces higher post velocity, and correspondingly lowers the energy dissipation. The good correlation between the energy loss coefficient and the maximum back facet deflection supports this interpretation. Aside from that, the stiff CFRP is easier to get ruptured first under large deformation. It dissipates great amount of impact energy and boosts the energy loss coefficient in Fig. 9.d. Fig. 10 (CT5,CH5) displays the damaged truss and hexagon panel for the moment when the impact energy is fully absorbed. It's evident that the whole panel scatters, and the impactor penetrates the back face sheet in the next loading. In contrast, the damaged re-entrant panel can sustain further impacts. Fig. 10 (CR4,CR5) is selected to show this process. Ruptured front face sheet rotates around the impactor and allows it to penetrate directly. But the intact core structure spreads the load as usual and congregates towards the impact location. Consequently, densified core bends with the back

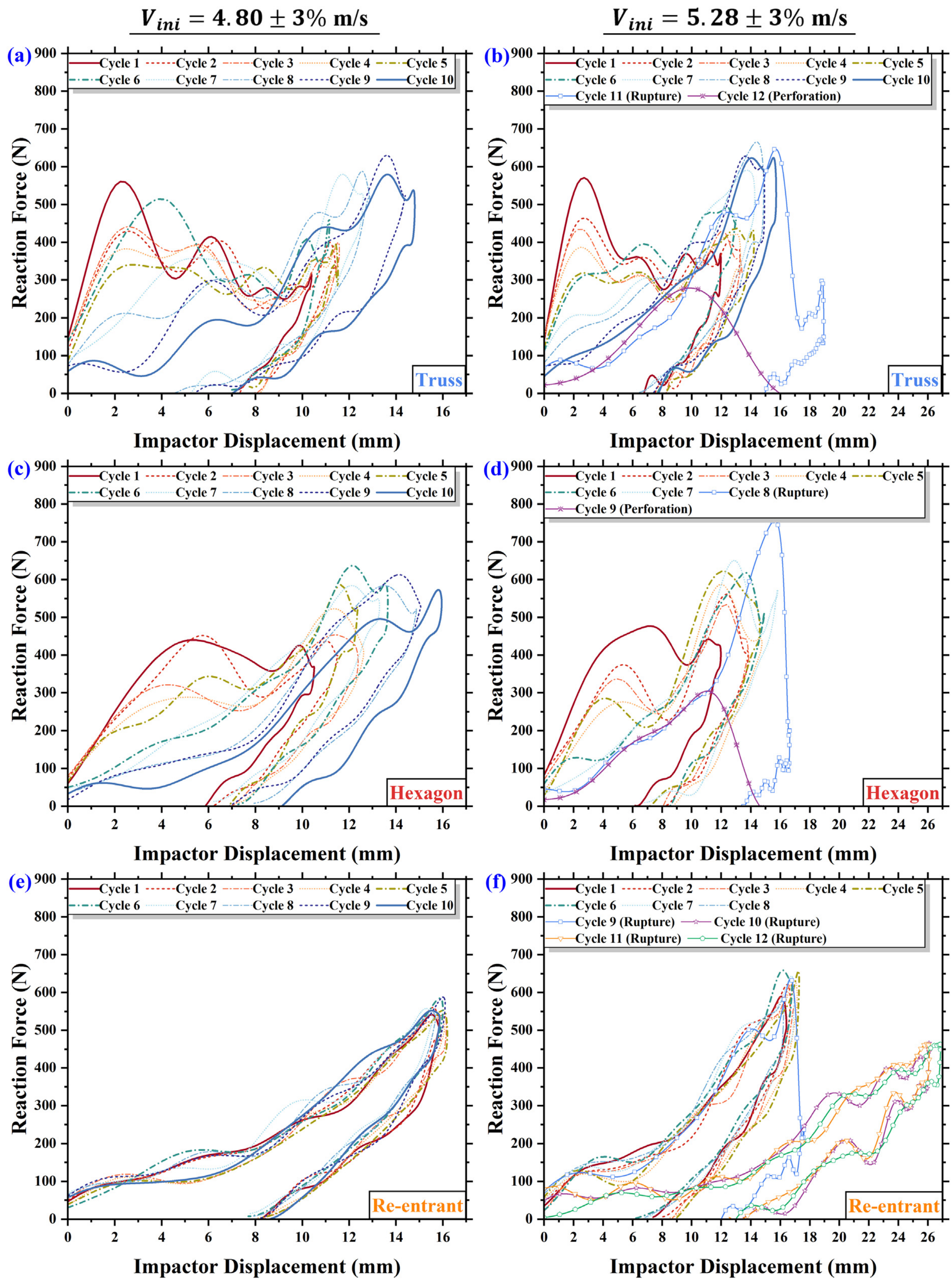

Fig. 8. Filtered reaction force versus impactor displacement from two cyclic impact velocities, $V_{ini} = 4.80 \pm 3\%$ m/s (medium, 3.84 J) and $V_{ini} = 5.28 \pm 3\%$ m/s (higher, 4.65 J). They are for (a,b) truss, (c,d) hexagon, and (e,f) re-entrant panel, respectively; samples in (b,d,f) fail in front face sheet rupture or panel perforation.

face sheet, producing larger deflection (Fig. 9.f). Furthermore, by comparing Fig. 10 (CR3,CR5), we find that those ligaments around the nose of the impactor suffer from extreme load and also fracture gradually. Thus, the energy loss coefficient decreases, and the perforation occurs eventually. However, further investigation reveals that the damaged re-entrant panel shows enduring energy dissipation

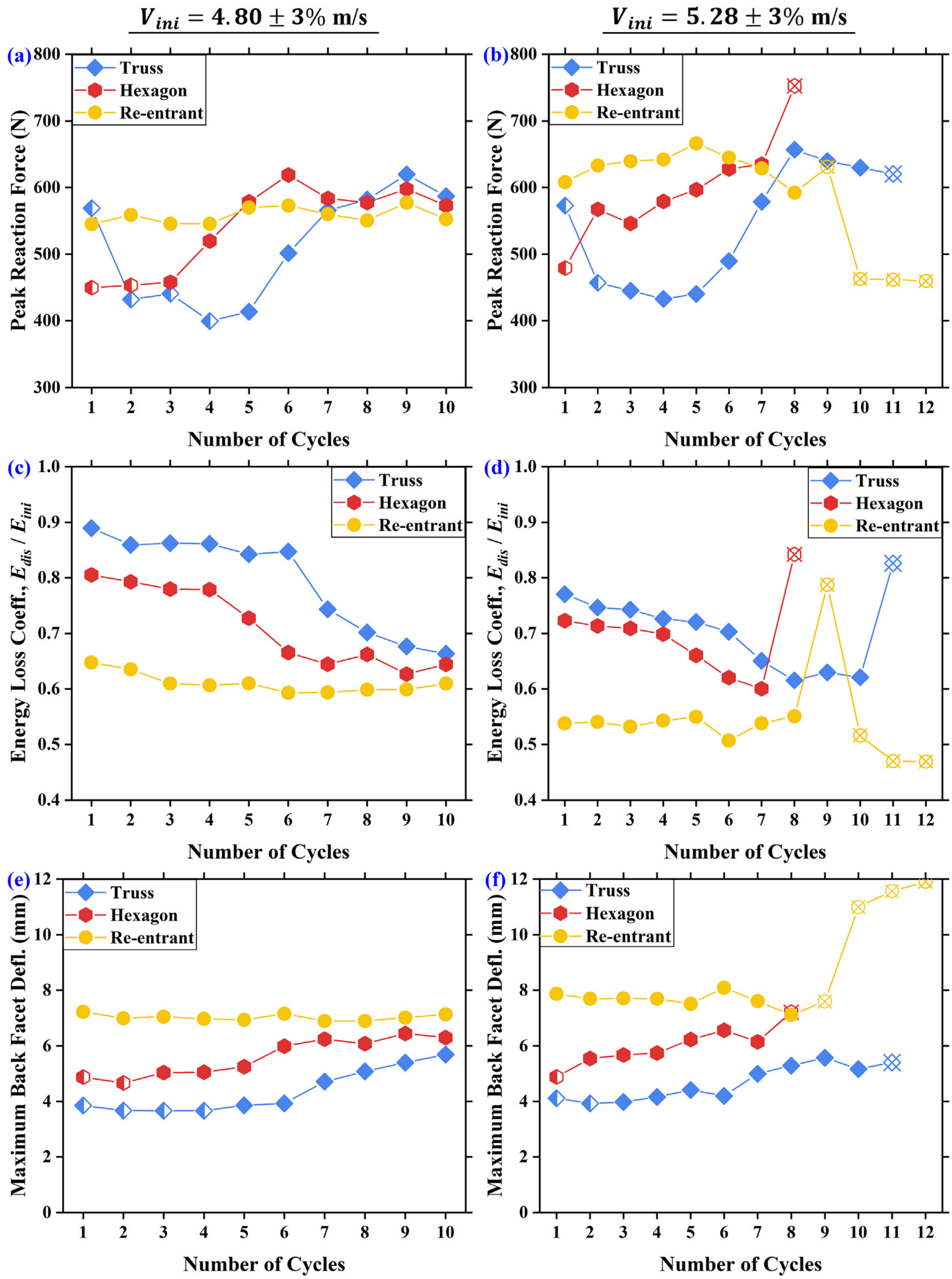

Fig. 9. Summarized three parameters from two cyclic impact velocities, $V_{ini} = 4.80 \pm 3\%$ m/s (medium, 3.84 J) and $V_{ini} = 5.28 \pm 3\%$ m/s (higher, 4.65 J). They are for (a,b) peak reaction force, (c,d) energy loss coefficient, and (e,f) maximum back face sheet deflection, respectively; crossed symbol indicates the front face sheet ruptures, and half-filled symbol means the value is found before core structure instability.

ability when loaded elsewhere, which is not the case for neither truss nor hexagon design. Detailed discussions will be presented in future works.

It appears that, even if the truss and hexagon core are progressively damaged, they still perform better or, at least, close to the intact re-entrant core. That is because we impacted them with relatively high energy to accelerate this degradation process. When appropriate impact energy is selected, such as the first region in Fig. 7, the re-entrant panel is anticipated to exhibit not only the lowest peak reaction force, similar energy loss coefficient and deflection,

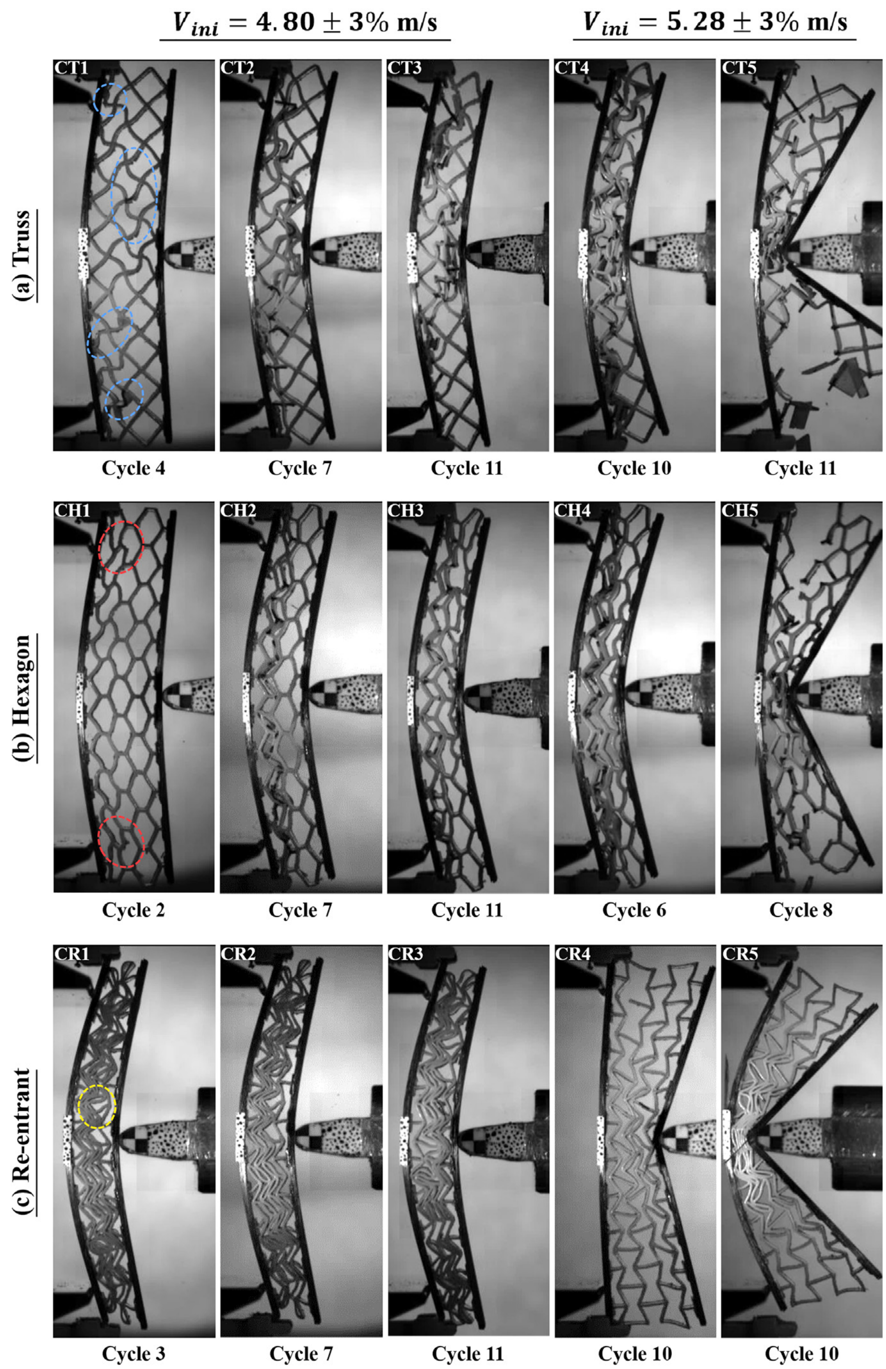

Fig. 10. Snapshots of the tested lattice composites under cyclic impact for truss (CT), hexagon (CH) and re-entrant (CR), respectively. First three columns are from impact velocity $V_{ini} = 4.80 \pm 3\%$ m/s (medium, 3.84 J) while last two are from $V_{ini} = 5.28 \pm 3\%$ m/s (higher, 4.65 J); They are for the moment when the peak reaction force occurs (CT1-3,CH1-3,CR1-3), when the impact energy is fully absorbed (CT4-5,CH4-5) and for demonstrating the deformation process of the damaged re-entrant panel (CR4-5).

but also stable performance. This superior reliability results from the durable re-entrant core, and fundamentally, benefits from employing the robust auxetic design. Unlike the meritorious force mitigation property [15,19,21], the reliable structure performance is pivotal to its interdisciplinary applications. The successful realization of the auxetic topology in vibration control (acoustics) [56], heat recovery (thermodynamics) [62], remote control (electromagnetism) [63] and stretchable electronics [64] all posts the requirement of high structural reliability.

4. Conclusion

Dynamic three-point bending tests are conducted to investigate the reliability of auxetic and non-auxetic lattice composites. Three types of core topologies, diamond lattice (truss), conventional honeycomb (hexagon) and re-entrant honeycomb (re-entrant), are compared. We first identify the divergent unit cell deformation pattern and then explore the influence of core structure robustness and durability.

For sustaining impact load, the re-entrant core folds cell walls, producing interlaced pattern globally, whereas both truss and hexagon buckle core ligaments, yielding localized hinge-rotation and snap-through phenomenon, respectively. This interlaced pattern is not good at absorbing energy compared with the other two but grants the re-entrant structure superior robustness and durability. Therefore, the re-entrant panel shows both low peak reaction force and high energy loss coefficient, provided that the impact energy is appropriate. However, as the energy increases, fully densified re-entrant core shall bend with two face sheets and raises the reaction force drastically. It not only lowers energy dissipation, but also yields large deflection and hence ruptures the face sheet earlier. Nevertheless, the robust re-entrant design stabilizes the penetration occurrence regardless of the impact energy, making the panel performance more predictable. Furthermore, the re-entrant core remains intact and performs remarkably consistent under cyclic impact. In contrast, both truss and honeycomb panel show progressively damaged core structures due to the stress concentration, which perturbs the peak force value and degrades the energy loss coefficient significantly. Aside from that, the durable core structure also brings the re-entrant panel better performance after penetration occurs while other two designs scatter immediately when the front face sheet ruptures.

These results aid in the elucidation of the applicability of these three core topologies. We hope they could inspire new class of auxetic lattice composites with enhanced mechanical performances, especially under cyclic loading condition, and facilitate multi-functional material applications.

Data availability

The raw/processed data required to reproduce these findings cannot be shared at this time as they also form an ongoing study. Part of the data will be made available on email request.

CRediT authorship contribution statement

Shaoyu Hou: Conceptualization, Data curation, Formal analysis, Investigation, Methodology, Software, Validation, Visualization, Writing - original draft, Writing - review & editing. **Tiantian Li:** Conceptualization, Investigation, Software, Validation, Writing - original draft, Writing - review & editing. **Zian Jia:** Data curation, Software, Writing - review & editing. **Lifeng Wang:** Funding acquisition, Investigation, Project administration, Resources, Supervision, Writing - review & editing.

Acknowledgments

The authors would like to acknowledge with much appreciation the support from the Office of Naval Research (Dr. Yapa Rajapakse, Solid Mechanics Program). S.H. is grateful to the encouragement from Prof. Toshio Nakamura and Prof. Qiaode Ge (State University of New York at Stony Brook).

Appendix A. Reaction force and face sheet deflection

We also summarized curves of the filtered and unfiltered reaction forces, displacement of the impactor, deflection of the back facet as well as their difference ΔU (lattice composite thickness reduction) into Fig. A.1. Those moments in Figs. 4 and 5 were marked accordingly. Unlike impactor displacement, all back face sheet deflection depicts a clear recovery trend. It indicates that the core structure instability occurs, but its influence is postponed by the inertial effect.

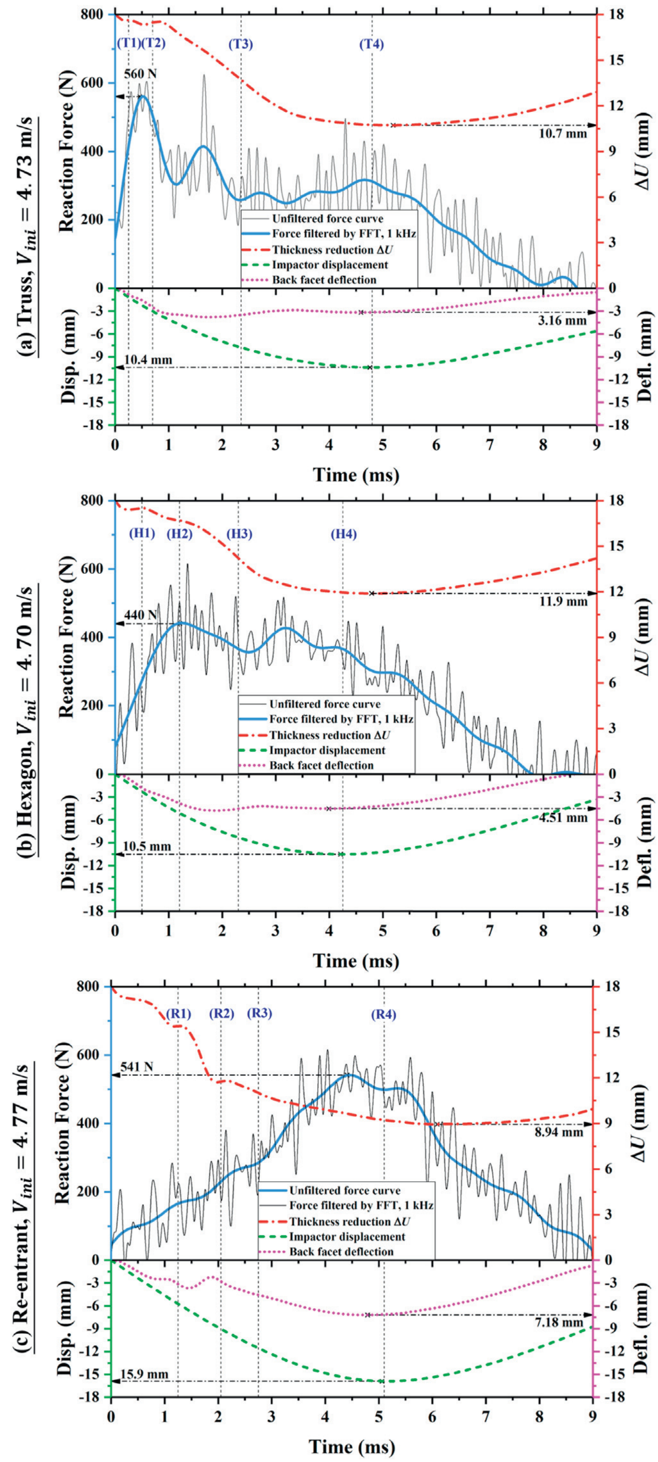

Fig. A.1. Curves of reaction force, impactor displacement, back facet deflection and their difference, ΔU, for truss, hexagon and re-entrant panel, respectively. Those moments in Fig. 5 are marked accordingly.

Those force trend discrepancies could be interpreted as follows. When the impact occurs, both truss and hexagon stably convey the impact load. The response force increases until it reaches the critical value (560 N and 440 N, respectively). Then two sandwich panels buckle core ligaments to suppress the transmitted load until the impact energy is fully dissipated, producing hinge-rotation or snap-through pattern. Since the hexagon structure diffuses the impact load (hence buckle) uniformly, it performs better in alleviating the peak response force. This can also be understood by examining the face sheet flexure in Fig. 5 (T2,H2). The straight front face sheet in the truss panel is the consequence of non-uniform sandwich core deformation, whereas two parallel face sheets from the hexagon panel suggest evenly distributed impact loads. In contrast, the re-entrant core is inherently unstable in sustaining impact load, exhibiting much lower flexural stiffness (Fig. 3.d). Those core ligaments fold with each other, which enhances structural integrity. This mechanism is reported to be the best in mitigating response force [20,21]. Nonetheless, our results indicate that its energy absorption capability is very limited. After the core structure fully densifies, it shall bend with two face sheets together, and the reaction force increases remarkably (541 N). It also explains why the re-entrant panel yields much larger impactor displacement (15.9 mm) and back face sheet deflection (7.18 mm) as well as a smaller ΔU value (8.94 mm). Accordingly, those three minor perturbations existing in the loading region could be interpreted. They are the consequence of ligament hinge contact (Fig. 5.R1), interlaced pattern (Fig. 5.R2) and ligaments buckling (Fig. 5.R3), respectively.

Appendix B. Characterizing the flexural stiffness of the face sheet

We also conducted low velocity impact tests on three face sheets to quantify their flexural stiffness. The dynamic test approach is the same as reported in Section 2.3. Fig. B.2.a displays the raptured CFRP face sheet, and Fig. B.2 (b–d) summarizes the reaction force curves from different incident velocities. As can be seen, these curves fluctuate heavily but show similar trend. Linear regression on their loading region indicates the flexural stiffness is 25.078 kN/m, 25.734 kN/m and 26.414 kN/m for three loading scenarios, respectively. Hence, the averaged value, 25.74 kN/m, is used to evaluate the energy collected by the two face sheets. Aside from that, the load where the face sheet ruptures (⩽ 400 N) is clearly lower than those recorded from lattice composites (≈750 N in Fig. 7.b). It aligns with the analysis in [50] and reveals the potential of employing embedded core structures. Additionally, those large perturbations during the unloading region in Fig. B.2.c may result from the macro-cracks when the sample approaches failure.

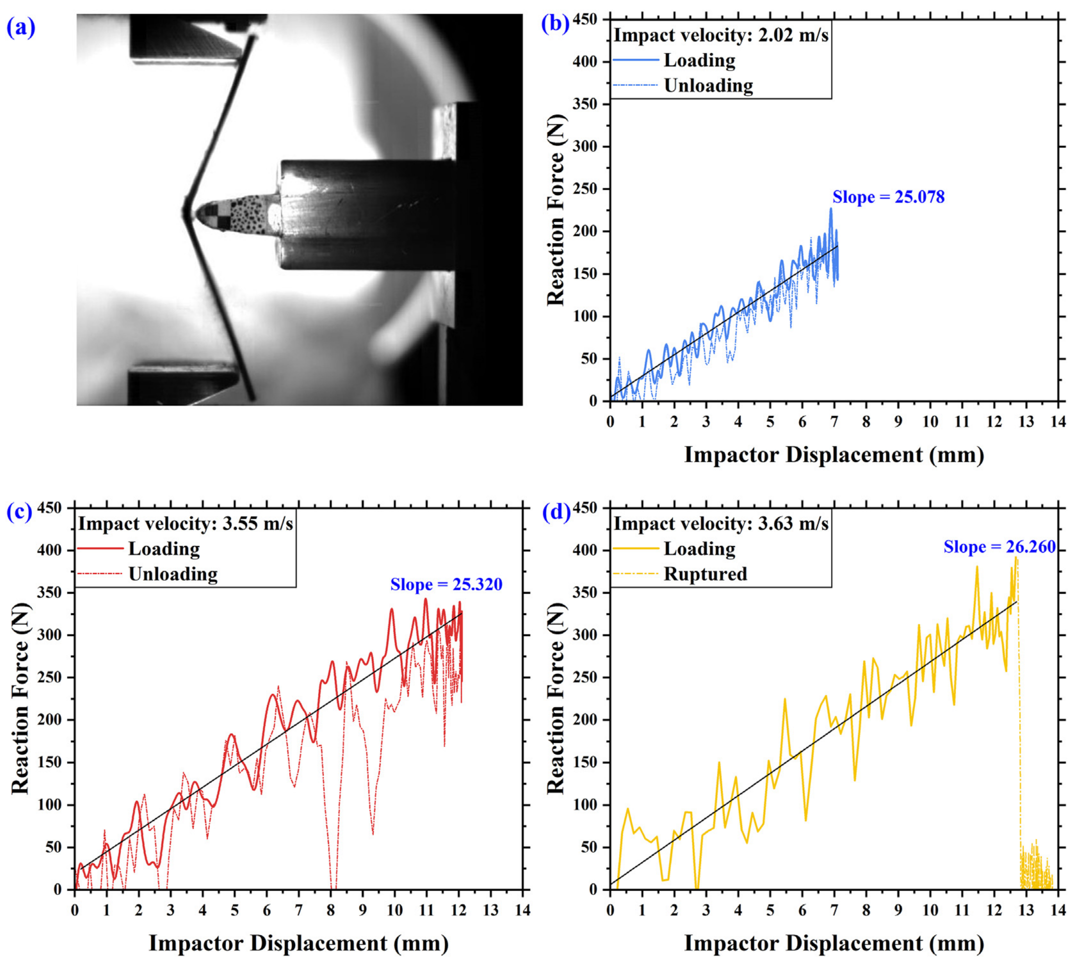

Fig. B.2. Face sheet impact test and unfiltered response force curves.

Appendix C. Panel performance under lower velocity cyclic impact

We also summarized the filtered reaction force curves and quantified three parameters for cyclic impact velocity, $V_{ini} = 4.29 \pm 3\%$ m/s (lower, 3.07 J). The force trends in Fig. C.3(a,c,e) are anticipated, but the damage evolution slows down since the impact energy is not too large. Therefore, the shifting trend postpones in Fig. C.3.b, and even the hexagon panel exhibits a decreasing peak force trend in the first few cycles. Furthermore, the lower impact velocity also makes sandwich panel performance more susceptible to the dynamic inertial effect, perturbing the peak force value slightly. But still, all the trends are similar to those observed in Fig. 9, and further validate our interpretations.

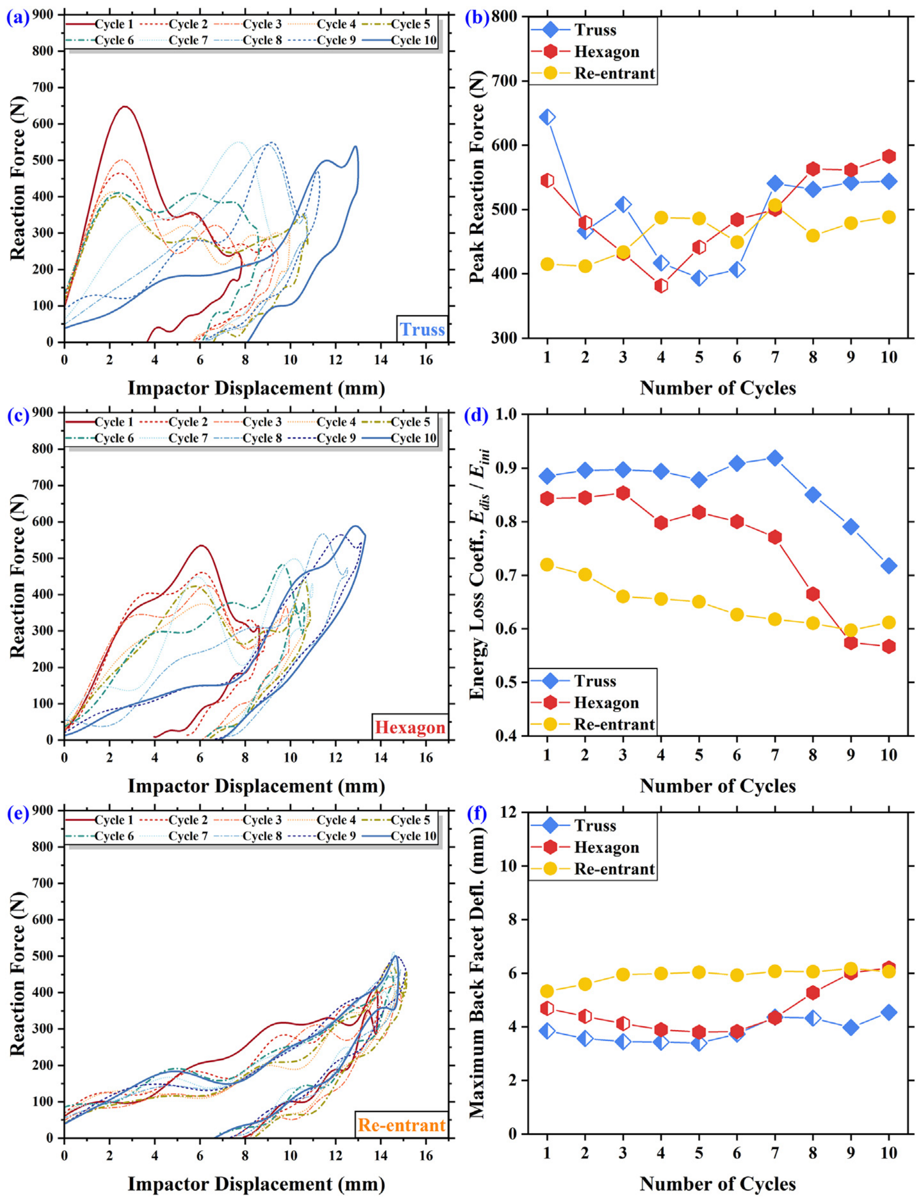

Fig. C.3. Filtered reaction force curves and summarized three parameters from cyclic impact velocity, $V_{ini} = 4.29 \pm 3\%$ m/s (lower, 3.07 J). Left three are for (a) truss, (c) hexagon, and (e) re-entrant panel, respectively; Right three compare the trend of (b) peak reaction force, (d) energy loss coefficient and (f) maximum back face sheet deflection; Half-filled symbol means the value is found before core structure instability.

References

[1] V. Birman, G.A. Kardomatea, Review of current trends in research and applications of sandwich structures, Compos. Part B Eng. (2018).
[2] R. Lakes, Foam structures with a negative Poisson's ratio, Science (1987) 1038–1040.
[3] L.J. Gibson, M.F. Ashby, G. Schajer, C. Robertson, The mechanics of two-dimensional cellular materials, Proc. R. Soc. Lond. A 382 (1782) (1982) 25–42.
[4] L. Yang, O. Harrysson, D. Cormier, H. West, C. Park, K. Peters, Design of auxetic sandwich panels for structural applications, Solid Freeform Fabrication Symposium, vol. 929, 2013.
[5] G. Imbalzano, P. Tran, T.D. Ngo, P.V. Lee, Three-dimensional modelling of auxetic sandwich panels for localised impact resistance, J. Sandw. Struct. Mater. 19 (3) (2017) 291–316.
[6] X. Jin, Z. Wang, J. Ning, G. Xiao, E. Liu, X. Shu, Dynamic response of sandwich structures with graded auxetic honeycomb cores under blast loading, Compos. Part B Eng. 106 (2016) 206–217.
[7] L. Boldrin, S. Hummel, F. Scarpa, D. Di Maio, C. Lira, M. Ruzzene, C. Remillat, T. Lim, R. Rajasekaran, S. Patsias, Dynamic behaviour of auxetic gradient composite hexagonal honeycombs, Compos. Struct. 149 (2016) 114–124.
[8] P. Vogiatzis, S. Chen, X. Wang, T. Li, L. Wang, Topology optimization of multi-material negative Poisson's ratio metamaterials using a reconciled level set method, Comput. Aided Des. 83 (2017) 15–32.
[9] T. Li, Y. Chen, X. Hu, Y. Li, L. Wang, Exploiting negative Poisson's ratio to design 3D-printed composites with enhanced mechanical properties, Mater. Des. 142 (2018) 247–258.
[10] K.E. Evans, A. Alderson, Auxetic materials: functional materials and structures from lateral thinking!, Adv. Mater. 12 (9) (2000) 617–628.
[11] F. Scarpa, L. Ciffo, J. Yates, Dynamic properties of high structural integrity auxetic open cell foam, Smart Mater. Struct. 13 (1) (2003) 49.
[12] L. Jiang, H. Hu, Low-velocity impact response of multilayer orthogonal structural composite with auxetic effect, Compos. Struct. 169 (2017) 62–68.
[13] T. Fíla, P. Zlámal, O. Jiroušek, J. Falta, P. Koudelka, D. Kytýř, T. Doktor, J. Valach, Impact testing of polymer-filled auxetics using split Hopkinson pressure bar, Adv. Eng. Mater. 19 (10) (2017).
[14] L.J. Gibson, M.F. Ashby, Cellular Solids: Structure and Properties, Cambridge university press. 1999.
[15] C. Qi, A. Remennikov, L.-Z. Pei, S. Yang, Z.-H. Yu, T.D. Ngo, Impact and close-in blast response of auxetic honeycomb-cored sandwich panels: experimental tests and numerical simulations, Compos. Struct. 180 (2017) 161–178.
[16] C. Qi, S. Yang, D. Wang, L.-J. Yang, Ballistic resistance of honeycomb sandwich panels under in-plane high-velocity impact, Sci. World J. 2013 (2013).
[17] W. Liu, N. Wang, T. Luo, Z. Lin, In-plane dynamic crushing of re-entrant auxetic cellular structure, Mater. Des. 100 (2016) 84–91.
[18] Z. Zhou, J. Zhou, H. Fan, Plastic analyses of thin-walled steel honeycombs with re-entrant deformation style, Mater. Sci. Eng. A 688 (2017) 123–133.
[19] T. Li, L. Wang, Bending behavior of sandwich composite structures with tunable 3D-printed core materials, Compos. Struct. 175 (2017) 46–57.
[20] H.Y. Sarvestani, A. Akbarzadeh, H. Niknam, K. Hermenean, 3D printed architected polymeric sandwich panels: energy absorption and structural performance, Compos. Struct. 200 (2018) 886–909.
[21] C. Yang, H.D. Vora, Y. Chang, Behavior of auxetic structures under compression and impact forces, Smart Mater. Struct. 27 (2) (2018) 025012.
[22] Z. Zou, S. Reid, P. Tan, S. Li, J. Harrigan, Dynamic crushing of honeycombs and features of shock fronts, Int. J. Impact Eng. 36 (1) (2009) 165–176.
[23] K. Kanny, H. Mahfuz, Flexural fatigue characteristics of sandwich structures at different loading frequencies, Compos. Struct. 67 (4) (2005) 403–410.
[24] M. Burman, D. Zenkert, Fatigue of foam core sandwich beams-1: undamaged specimens, Int. J. Fatigue 19 (7) (1997) 551–561.
[25] F. Yang, Q. Lin, J. Jiang, Experimental study on fatigue failure and damage of sandwich structure with PMI foam core, Fatigue Fract. Eng. Mater. Struct. 38 (4) (2015) 456–465.
[26] B. Shafiq, A. Quispitupa, Fatigue characteristics of foam core sandwich composites, Int. J. Fatigue 28 (2) (2006) 96–102.
[27] A. Chemami, K. Bey, J. Gilgert, Z. Azari, Behaviour of composite sandwich foam-laminated glass/epoxy under solicitation static and fatigue, Compos. Part B Eng. 43 (3) (2012) 1178–1184.
[28] D. Zenkert, M. Burman, Tension, compression and shear fatigue of a closed cell polymer foam, Compos. Sci. Technol. 69 (6) (2009) 785–792.
[29] S. Clark, R. Shenoi, H. Allen, Modelling the fatigue behaviour of sandwich beams under monotonic, 2-step and block-loading regimes, Compos. Sci. Technol. 59 (4) (1999) 471–486.
[30] S.M. Soni, R.F. Gibson, E.O. Ayorinde, The influence of subzero temperatures on fatigue behavior of composite sandwich structures, Compos. Sci. Technol. 69 (6) (2009) 829–838.
[31] E. Bozhevolnaya, O.T. Thomsen, Structurally graded core junctions in sandwich beams: fatigue loading conditions, Compos. Struct. 70 (1) (2005) 12–23.
[32] D. Zenkert, M. Burman, Failure mode shifts during constant amplitude fatigue loading of GFRP/foam core sandwich beams, Int. J. Fatigue 33 (2) (2011) 217–222.
[33] M. Burman, D. Zenkert, Fatigue of foam core sandwich beams-2: effect of initial damage, Int. J. Fatigue 19 (7) (1997) 563–578.
[34] B. Freeman, E. Schwingler, M. Mahinfalah, K. Kellogg, The effect of low-velocity impact on the fatigue life of sandwich composites, Compos. Struct. 70 (3) (2005) 374–381.
[35] N. Sharma, R.F. Gibson, E.O. Ayorinde, Fatigue of foam and honeycomb core composite sandwich structures: a tutorial, J. Sandw. Struct. Mater. 8 (4) (2006) 263–319.
[36] A. Bezazi, F. Scarpa, Mechanical behaviour of conventional and negative Poisson's ratio thermoplastic polyurethane foams under compressive cyclic loading, Int. J. Fatigue 29 (5) (2007) 922–930.
[37] A. Bezazi, F. Scarpa, Tensile fatigue of conventional and negative Poisson's ratio open cell PU foams, Int. J. Fatigue 31 (3) (2009) 488–494.
[38] J. Lisiecki, D. Nowakowski, P. Reymer, Fatigue properties of polyurethane foams, with special emphasis on auxetic foams, used for helicopter pilot seat cushion inserts, Fatigue Aircr. Struct. 2014 (6) (2014) 72–78.
[39] L. Zhou, J. Zeng, L. Jiang, H. Hu, Low-velocity impact properties of 3D auxetic textile composite, J. Mater. Sci. 53 (5) (2018) 3899–3914.
[40] Y.-M. Jen, L.-Y. Chang, Evaluating bending fatigue strength of aluminum honeycomb sandwich beams using local parameters, Int. J. Fatigue 30 (6) (2008) 1103–1114.
[41] Y.-M. Jen, C.-W. Ko, H.-B. Lin, Effect of the amount of adhesive on the bending fatigue strength of adhesively bonded aluminum honeycomb sandwich beams, Int. J. Fatigue 31 (3) (2009) 455–462.
[42] Y.-M. Jen, L.-Y. Chang, Effect of thickness of face sheet on the bending fatigue strength of aluminum honeycomb sandwich beams, Eng. Fail. Anal. 16 (4) (2009) 1282–1293.
[43] S. Belouettar, A. Abbadi, Z. Azari, R. Belouettar, P. Freres, Experimental investigation of static and fatigue behaviour of composites honeycomb materials using four point bending tests, Compos. Struct. 87 (3) (2009) 265–273.
[44] A. Abbadi, Z. Azari, S. Belouettar, J. Gilgert, P. Freres, Modelling the fatigue behaviour of composites honeycomb materials (aluminium/aramide fibre core) using four-point bending tests, Int. J. Fatigue 32 (11) (2010) 1739–1747.
[45] A. Abbadi, C. Tixier, J. Gilgert, Z. Azari, Experimental study on the fatigue behaviour of honeycomb sandwich panels with artificial defects, Compos. Struct. 120 (2015) 394–405.
[46] G. Bianchi, G.S. Aglietti, G. Richardson, Static and fatigue behaviour of hexagonal honeycomb cores under in-plane shear loads, Appl. Compos. Mater. 19 (2) (2012) 97–115.
[47] G. Belingardi, P. Martella, L. Peroni, Fatigue analysis of honeycomb-composite sandwich beams, Compos. A: Appl. Sci. Manuf. 38 (4) (2007) 1183–1191.
[48] W. Boukharouba, A. Bezazi, F. Scarpa, Identification and prediction of cyclic fatigue behaviour in sandwich panels, Measurement 53 (2014) 161–170.
[49] A. Rajaneesh, Y. Zhao, G. Chai, I. Sridhar, Flexural fatigue life prediction of CFRP-Nomex honeycomb sandwich beams, Compos. Struct. 192 (2018) 225–231.
[50] I.M. Daniel, J.L. Abot, Fabrication, testing and analysis of composite sandwich beams, Compos. Sci. Technol. 60 (12-13) (2000) 2455–2463.
[51] J.-S. Huang, S.-Y. Liu, Fatigue of honeycombs under in-plane multiaxial loads, Mater. Sci. Eng. A 308 (1-2) (2001) 45–52.
[52] G. Schaffner, X.-D.E. Guo, M.J. Silva, L.J. Gibson, Modelling fatigue damage accumulation in two-dimensional Voronoi honeycombs, Int. J. Mech. Sci. 42 (4) (2000) 645–656.
[53] L. Liu, J. Holmes, Experimental investigation of fatigue crack growth in thin-foil Ni-base sandwich structures, Int. J. Fatigue 29 (8) (2007) 1452–1464.
[54] O. Duncan, T. Shepherd, C. Moroney, L. Foster, P. Venkatraman, K. Winwood, T. Allen, A. Alderson, Review of auxetic materials for sports applications: expanding options in comfort and protection, Appl. Sci. 8 (6) (2018).
[55] D. Plant, Armourgel - smart, high impact armour for the older generation, https://www.youtube.com/watch?v=cUUCgASD9_M#t=1m00s.
[56] Y. Chen, T. Li, F. Scarpa, L. Wang, Lattice metamaterials with mechanically tunable Poisson's ratio for vibration control, Phys. Rev. Appl. 7 (2) (2017) 024012.
[57] Z. Jia, T. Li, F.-p. Chiang, L. Wang, An experimental investigation of the temperature effect on the mechanics of carbon fiber reinforced polymer composites, Compos. Sci. Technol. 154 (2018) 53–63.
[58] J. Yu, E. Wang, J. Li, Z. Zheng, Static and low-velocity impact behavior of sandwich beams with closed-cell aluminum-foam core in three-point bending, Int. J. Impact Eng. 35 (8) (2008) 885–894.
[59] T.A. Schaedler, A.J. Jacobsen, A. Torrents, A.E. Sorensen, J. Lian, J.R. Greer, L. Valdevit, W.B. Carter, Ultralight metallic microlattices, Science 334 (6058) (2011) 962–965.
[60] T. Allen, J. Shepherd, T. Hewage, T. Senior, L. Foster, A. Alderson, Low-kinetic energy impact response of auxetic and conventional open-cell polyurethane foams, Phys. Status Solidi B 252 (7) (2015) 1631–1639.
[61] J. Lisiecki, T. Błażejewicz, S. Kłysz, G. Gmurczyk, P. Reymer, G. Mikułowski, Tests of polyurethane foams with negative Poisson's ratio, Phys. Status Solidi B 250 (10) (2013) 1988–1995.
[62] J. Rossiter, K. Takashima, F. Scarpa, P. Walters, T. Mukai, Shape memory polymer hexachiral auxetic structures with tunable stiffness, Smart Mater. Struct. 23 (4) (2014) 045007.
[63] Y. Kim, H. Yuk, R. Zhao, S.A. Chester, X. Zhao, Printing ferromagnetic domains for untethered fast-transforming soft materials, Nature 558 (7709) (2018) 274.
[64] Y. Jiang, Z. Liu, N. Matsuhisa, D. Qi, W.R. Leow, H. Yang, J. Yu, G. Chen, Y. Liu, C. Wan, et al. Auxetic mechanical metamaterials to enhance sensitivity of stretchable strain sensors, Adv. Mater. 30 (12) (2018) 1706589.